Environ. Sci. Technol. **2005**, *39,* 6516−6526

Phenanthrene and Pyrene Sorption and Intraparticle Diffusion in Polyoxymethylene, Coke, and Activated Carbon†

SUNGWOO AHN,‡ DAVID WERNER,§ HRISSI K. KARAPANAGIOTI,|| DONALD R. MCGLOTHLIN,⊥ RICHARD N. ZARE,⊥ AND RICHARD G. LUTHY*,‡

Department of Civil and Environmental Engineering, Stanford University, Stanford, California 94305-4020, School of Civil Engineering and Geosciences, University of Newcastle upon Tyne, United Kingdom, Marine Science Department, University of the Aegean at Mytilene, Greece, and Department of Chemistry, Stanford University, Stanford, California 94305-5080

We report sorption isotherms and uptake kinetics for phenanthrene and pyrene with three organic model sorbents: polyoxymethylene (POM), coke, and activated carbon. We combine batch equilibration and kinetic experiments with the direct observation of the long-term diffusion of phenanthrene and pyrene as measured within cross-sectioned particles using microprobe laser-desorption laser-ionization mass spectroscopy (μL^{2}MS). For POM pellets, the intraparticle concentration profiles predicted from kinetic batch experiments and a polymer diffusion model with spherical geometry are in agreement with the independent μL^{2}MS measurements. For coke particles, the apparent diffusivities decreased with smaller particle size. These trends in diffusivities were described by a sorption-retarded pore diffusion model with a particle-size-dependent solid−water partitioning coefficient obtained from apparent equilibrium observed in the kinetic batch studies. For activated carbon, the μL^{2}MS measurements showed faster radial diffusion of phenanthrene and pyrene into the particle interior than predicted from diffusion models based on a single sorption domain and diffusivity. A branched pore kinetic model, comprising polycyclic aromatic hydrocarbon (PAH) macropore diffusion with kinetic exchange of PAH between macroporous and microporous domains, fits the experimental observations better. Because of parallel macro- and microdiffusion processes, nonlinear sorption isotherms, and a concentration-dependent diffusivity, it is not possible to make independent parameter estimations for intraparticle diffusion in activated carbon using our present procedures.

Introduction

Carbon-rich materials are strong sorbents for polycyclic aromatic hydrocarbons (PAHs) and other hydrophobic chemicals from aqueous solutions (*1*). These sorbent materials play an important role in the natural environment, where the availability of PAHs and similar hydrophobic contaminants is critically related to the amount, structure, and nature of heterogeneous carbonaceous matter (*2*−*4*). The observation of strong contaminant sequestration by carbon-rich materials results in the use of such materials in engineering applications in the field, including use as sorptive walls for groundwater cleanup (*5*) and as a proposed amendment to reduce contaminant bio-uptake from sediment (*6*−*8*).

For PAHs and other hydrophobic chemicals, extensive research has refined the conceptual description of the distribution equilibrium between the aqueous phase and carbonaceous sorbents as outlined by Allen-King et al. (*9*) and the more than 170 references therein. It is generally accepted that carbonaceous sorbents may exhibit at least two distinct sorption domains: an "organic", "soft", "soft polymeric", or "gel-like" carbonaceous matrix that is associated with linear sorption isotherms and a "black", "hard", "glassy polymeric", and/or "microporous" domain that exhibits nonlinear sorption isotherms (*10*−*14*). In the first case, the carbonaceous material is assumed to be flexible enough to accommodate a solute in a fashion similar to its dissolution in a liquid organic solvent, and therefore a linear sorption isotherm is generally well-correlated with solvent−solvent partitioning coefficients, e.g., the octanol−water partitioning coefficient, K_{ow}. In the second case, the carbonaceous matrix is perceived to be much more rigid, and sorption presumably occurs on surfaces and within existing molecular-sized cavities or micropores. The number of such sorption sites is limited, and the potential for energetic interaction is variable, depending on the shape and size of the molecule and the cavity. Consequently, the measured sorption isotherms are nonlinear. Furthermore, the sorption in such molecular-sized cavities appears to be exceptionally strong, resulting in much higher solid−aqueous phase partitioning coefficients than anticipated from solvent−solvent partitioning, especially at low aqueous concentrations (*9*).

For hydrophobic chemicals such as PAHs and a strong sorbent, the partitioning between the aqueous and the solid phase is often controlled by slow sorption kinetics (*15*, *16*). It is generally understood that the slow sorption kinetics are caused by rate-limiting diffusive mass transfer (*17*−*19*). Proposed models for the mechanism of slow sorption include sorption-retarded diffusion in pores (*17*, *20*), surface diffusion along pore walls (*21*), or diffusion in a polymeric matrix (*18*). Diffusion-based models are widely used to interpret sorption and/or desorption processes from batch or column experiments with model sorbents and natural sediments (*2*, *19*, *22*−*27*). However, investigations with complex carbonaceous sorbents reveal significant discrepancies with the predictions of diffusion-based models, which are attributed variously to uncertainties about the length scale of diffusion (*19*) or different diffusional mechanisms in micro- versus meso- and macropores (*24*, *25*, *28*). These conceptualizations and interpretations are based on the rate of change of sorbate concentrations measured in the external bulk phase.

The purpose of this study is to investigate the equilibrium and kinetics of PAH sorption to organic sorbents. For this study, we chose phenanthrene and pyrene as sorbates. We

† This paper is part of the Charles O'Melia tribute issue.

* Corresponding author phone: (650)723-3921; fax: (650)725-8662; e-mail: luthy@stanford.edu.

‡ Department of Civil and Environmental Engineering, Stanford University.

§ University of Newcastle upon Tyne.

|| University of the Aegean at Mytilene.

⊥ Department of Chemistry, Stanford University.

10.1021/es050113o CCC: $30.25
Published on Web 07/14/2005

selected polyoxymethylene (POM) pellets as a model for a flexible polymeric sorbent matrix, coke breeze as an example of a thermally altered, black carbon particle, and activated carbon as a model sorbent comprising a microporous, carbon-derived material. We combine an array of traditional batch experiments with the direct observation of the long-term diffusion inside cross-sectioned particles as measured at a 40-μm scale with microprobe laser-desorption laser-ionization mass spectroscopy (μL^{2}MS). While our results confirm many of the qualitative predictions of diffusion-based sorption models, we demonstrate the complexity of the actual diffusion process, especially for coke and activated carbon.

Materials and Methods

Chemicals and Sorbents. Phenanthrene and pyrene were purchased as pure compounds (Aldrich, Milwaukee, WI). Polyoxymethylene pellets with 2−3-mm diameters were purchased from Aldrich (Milwaukee, WI). They were used as purchased without precleaning for physical property measurements. Otherwise, they were boiled in deionized water for 30 min prior to use. Precleaning using solvent was avoided because soaking in a solvent swells the polymeric matrix and may result in matrix heterogeneity if residual solvent is trapped in the pellets. For kinetic experiments, a number of pellets were cut with a razor blade into smaller particles (1.5-mm diameter), and for sorption equilibrium experiments, they were sliced into disks of approximately 0.25 mm in thickness. Coke breeze (coke) obtained from Ispat Inland, Inc. (East Chicago, IN) was crushed, washed, and wet-sieved into 1−5-, 0.11−0.25-, and 0.06−0.11-mm sieve fractions for kinetic experiments, and coke was pulverized for sorption equilibrium experiments (particle diameter <0.063 mm). The 10 × 30 MRX activated carbon (AC) was obtained from Calgon Carbon Corporation (Pittsburgh, PA), crushed, washed, and wet-sieved into 1−2-, 0.25−0.58-, and 0.06−0.25-mm sieve fractions for kinetic experiments, and AC was pulverized for sorption equilibrium experiments. Brunauer−Emmett−Teller surface areas (BET-SAs), pore size distributions, and pore volumes were measured with N_2 adsorption at 77 K using a COULTER SA 3100 surface area and pore size analyzer (Coulter Corporation, Miami, FL). The total porosity of the coarsest sorbent fraction was determined from the water content of the sorbent after boiling for 30 min in water and rolling on paper towels to remove external water films (*1*). Solid density was determined according to American Society for Testing and Materials method D854. Total organic carbon of the various fractions was determined by combustion and elemental analysis of acidified samples (*29*).

Sorption Isotherms and Kinetic Experiments. Experiments were conducted in triplicates using previously described procedures (*15*), as outlined in the Supporting Information. Aqueous phenanthrene and pyrene concentrations in batches with sorbent materials were measured by fluorescence. The distribution between the solid and the aqueous phase was calculated based on the total PAH mass in the batches and monitored as a function of time. For each batch experiment, triplicate blank control samples with phenanthrene or pyrene solutions and without sorbent were prepared and monitored. Initial concentrations were calculated based on these measurements. Triplicate blank samples with sorbent and synthetic water only were monitored for desorption of natively bound solutes. However, no measurable concentrations of phenanthrene or pyrene were detected in the solution.

Sample Preparation for μL^{2}MS Measurements. In batch uptake experiments, particles were exposed to either a fixed amount or an unlimited supply of PAH sorbates. In the first case, individual sorbent particles were exposed in continuously rotated batches with a nearly saturated aqueous solution of phenanthrene or phenanthrene and pyrene (0.6 and 0.05 mg/L respectively), as described in the Supporting Information. In the second case, an air-bridge system configuration used by Bucheli and Gustafsson (*30*) was adapted for the exposure of sorbent particles in a system with an unlimited supply of PAHs. At sampling times, sorbent particles were removed from the vials or the air-bridge system with forceps and dried externally on a paper towel. Samples for μL^{2}MS analysis were prepared two ways. In the first, coke and activated carbon particles were embedded in a plaster, and shavings were cut from the solidified core until a clean cross section of the particle was exposed. In later experiments, POM or activated carbon particles were fixed with forceps and sectioned across the center with a razor blade on double-stick tape.

Intraparticle μL^{2}MS Measurements. Microprobe two-step laser-desorption laser-ionization mass spectrometry (μL^{2}MS), as described in the Supporting Information, was used to observe the diffusion of PAHs within the interior of sectioned particles. Clean, razor-cut POM, coke, and AC particles were scanned for background signals with μL^{2}MS. Mass spectrometer signals at 178 amu (phenanthrene) and 202 amu (pyrene) could be detected on coke particles, when the instrument was optimized for sensitivity but were barely above the detection limit and did not affect interpretation of our diffusion results. For PAH-exposed and sectioned particles, laser shots were initiated first off the edge of the particle to quantify the background chamber signal intensity, and then shots were moved in 40-μm increments toward the particle center and continued in the same direction until the opposite edge of the particle was reached. Cross sections were measured close to the shortest diameter of a sectioned particle. In addition, signal intensities (50-shot average) were measured on the outer surface of each particle at different locations.

Results and Discussion

Sorbent Properties. Table 1 summarizes the physicochemical properties of the sorbents used in this study. Polyoxymethylene (POM), a rubbery or "soft" polymer at room temperature, served as a model for an amorphous sorbent that accommodates the PAHs within its polymeric matrix. POM pellets have a smooth exterior surface and a few small bubble-shaped cavities in the particle interior, probably from gas entrapment during molding.

Coke breeze (coke), a byproduct of coke production, was investigated as an example for a thermally altered, black carbon particle. SEM images (Figure S1a in the Supporting Information) reveal a spongelike structure with large, bubblelike macropores, while further magnification shows surface fractures. Most of the available BET-SA is located internally in the macropore space. The smooth external surface area of a spherical coke particle with a diameter of 1 mm is 0.005 m^2/g and for particles with a diameter of 0.06 mm is 0.09 m^2/g, clearly less than the BET-SAs of 0.7−5.8 m^2/g reported in Table 1. A particle-size dependency was observed for the N_2-adsorption isotherms (Figure S2 in the Supporting Information) and thus for the BET-SA as reported in Table 1. Also, although very small, the meso- and micropore volumes increase somewhat with particle-size reduction.

Activated carbon (AC) was investigated as a model for a microporous sorbent with high surface area. SEM images (Figures S1b and S3 in the Supporting Information) show some large, fracturelike macropores as well as regions on the AC particles comprising areas with a comparably compact matrix and other areas with large fragmentation. Contrary to the experiments with coke, no particle-size dependency was observed for parameters derived from the N_2-adsorption isotherms. A more detailed discussion of sorbent properties can be found in the Supporting Information.

TABLE 1. Sorbent Properties

	grain size (diameter) (cm)	f_{oc} (g/g)	solid density[a] (g/cm^3)	porosity[b] (cm^3/cm^3)	total pore volume[b] (cm^3/g)	mesopore volume[c] (cm^3/g)	micropore volume[d] (cm^3/g)	BET-SA[e] (m^2/g)
POM	0.2−0.3	0.40[f]	1.3 ± 0.1	0.01 ± 0.01	0.01 ± 0.01	0.01 ± 0.01	±0	(0.0 ± 0.1)
coke	0.1−0.5	0.90	1.7 ± 0.1	0.31 ± 0.04	0.27 ± 0.01	0.01 ± 0.01	±0	0.7 ± 0.2
	0.011−0.025					0.01 ± 0.01	$10^{-4} \pm 10^{-4}$	2.2 ± 0.7
	0.006−0.011					0.01 ± 0.01	$10^{-4} \pm 10^{-4}$	3.0 ± 1.0
	<0.006					0.02 ± 0.01	$3 \times 10^{-4} \pm 3 \times 10^{-4}$	5.8 ± 2.5
activated carbon	0.1−0.2	0.77	1.7 ± 0.1	0.49 ± 0.01	0.57 ± 0.03	0.47 ± 0.09	0.23 ± 0.03	754 ± 120
	0.025−0.058					0.49	0.23	833
	0.006−0.025					0.49	0.22	830

[a] From pycnometry. [b] From pore water volume, includes the macropores. [c] From N_2 adsorbed at $P_s/P_0 = 0.98$; includes micropores and does not include the macropores. [d] From N_2-adsorption isotherms with t-plot analysis. [e] From N_2-adsorption isotherms; isotherms were type I for AC, type II for coke, and type III for POM. [f] Calculated from chemical formula (−CH_2O−).

TABLE 2. Isotherm Parameters for POM, Coke, and Activated Carbon

	K_{POM}[a] ± 95% CI[b] (cm^3/g)	log K_{oc}[c]	log K_{ow}[d]
	Finely Sliced POM		
phenanthrene	$4.7 \times 10^3 \pm 300$	4.1	4.6
pyrene	$1.2 \times 10^4 \pm 1000$	4.5	5.2

	K^*_{Fr}[e] (g/g)	K^*_{Fr}[f] (mol/m^2 BET-SA)	K^*_{Fr}[g] (cm^3 sorbate PAH/cm^3 N_2 adsorbed at $P_s/P_0 = 0.98$)	1/n[h]
		Pulverized Coke		
phenanthrene	$3.5 \times 10^{-3} \pm 6 \times 10^{-4}$	3.4×10^{-6}	0.17	0.39 ± 0.06
pyrene	$1.8 \times 10^{-3} \pm 2 \times 10^{-4}$	1.5×10^{-6}	0.11	0.22 ± 0.04
		Pulverized AC		
phenanthrene	0.26 ± 0.02	1.8×10^{-6}	0.52	0.21 ± 0.02
	0.34 ± 0.12[i]			0.27 ± 0.08[i]
pyrene	0.11 ± 0.02	6.6×10^{-7}	0.27	0.31 ± 0.04
	0.13 ±0.04[i]			0.34 ± 0.08[i]
		Literature Values, Lignite Coke (*36*)		
phenanthrene	0.13	2.4×10^{-6}	0.60	0.24
		Literature Values, F100 Activated Carbon (*36*)		
phenanthrene	1.7	1.2×10^{-5}	3.9[j]	0.51
		Literature Values, F400 Activated Carbon (*32*)		
phenanthrene	0.30	1.7×10^{-6}	*k*	0.41
pyrene	0.17	8.5×10^{-7}	*k*	0.39

[a] K_{POM}, linear solid−water distribution coefficient for POM. [b] CI, confidence interval based on triplicate samples. [c] K_{oc}, organic carbon fractional content normalized solid−water distribution coefficient. [d] K_{ow}, octanol−water partition coefficient (*32*). [e,f,g] K^*_{Fr}, normalized Freundlich sorption constant for solid-phase concentrations expressed as either g/g, mol/m^2 BET-SA, or cm^3 sorbate PAH/cm^3 N_2 adsorbed at $P_s/P_0 = 0.98$; aqueous concentrations were normalized by the solubility of the solid PAH at 25 °C which is 1.29 mg/L for phenanthrene and 0.135 mg/L for pyrene (*32*) and the molar volume is 199 cm^3/mol for phenanthrene and 214 cm^3/mol for pyrene (*39*). [h] $N = 1/n$, Freundlich exponent. [i] Fitted for the lower concentration range. [j] The Freundlich isotherm, fitted over a wide concentration range of aqueous phenanthrene concentrations C_e/S, overestimates the maximum sorption capacity. [k] Not available.

Sorption Equilibrium. Figure 1 presents the isotherm data for phenanthrene and pyrene with finely sliced POM (Figure 1a), pulverized coke (Figure 1b), and pulverized AC (Figure 1c). POM isotherms were linear over the whole concentration range as expected (*14*, *31*). The distribution coefficient between POM and water, K_{POM}, was 4700 ± 300 L/kg for phenanthrene and 12000 ± 1000 L/kg for pyrene. This is approximately a factor of 2 larger than values reported elsewhere (*14*, *31*) for similar materials, which is probably a result of the POM used in this study originating from a different provider and being molded into resin instead of sheets.

Sorption isotherms for coke and AC were nonlinear and were fitted with the Freundlich model, providing the necessary input constants for the sorption kinetic models used. The Langmuir model with a single affinity did not fit the data well, as shown in Figure S4 in the Supporting Information, indicating that PAHs adhere to heterogeneous sorption sites with different affinities for the solutes. Aqueous PAH concentrations (C_w) were normalized by the aqueous solubility (S) of the solid PAHs (1.29 mg/L for phenanthrene and 0.135 mg/L for pyrene (*32*)).

$$q_s = K^*_{Fr}\left(\frac{C_w}{S}\right)^{1/n} \quad (1)$$

where q_s denotes the PAH concentration on the solid (g/g), K^*_{Fr} the normalized Freundlich coefficient, and $1/n$ the Freundlich exponent. Figures 1b and 1c present the fitted normalized Freundlich sorption isotherms, and Table 2 provides the corresponding isotherm parameters. The normalized Freundlich coefficient K^*_{Fr} is equal to the amount of solute that would sorb at the solubility limit. Dividing by the BET-SA shows that the compound-specific K^*_{Fr} values for

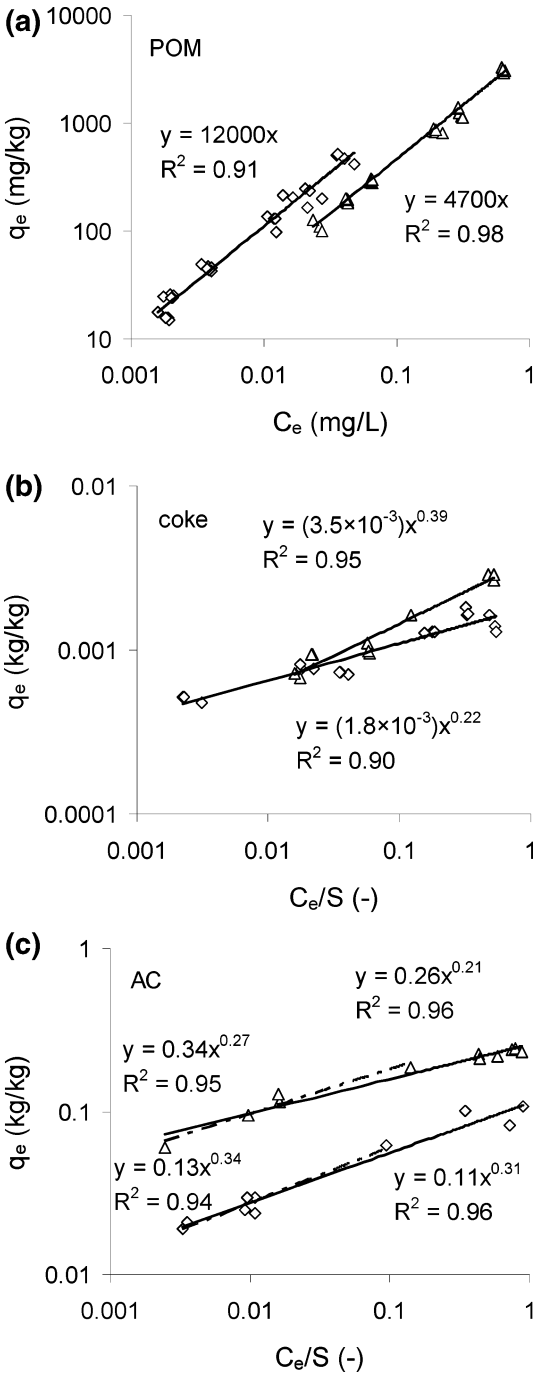

FIGURE 1. Sorption isotherms for phenanthrene (triangles) and pyrene (diamonds) on (a) polyoxymethylene, (b) coke, and (c) activated carbon. The fitting parameters for the Freundlich isotherms are provided in Table 2. For activated carbon, the Freundlich isotherm was fitted also for the lower concentration range only (broken line).

coke and AC are comparable within a factor of 2−3. For coke and AC, the amount of pyrene adsorbed is 50−70% less than the amount of phenanthrene adsorbed. Apparently, less of the BET-SA or pore space is accessible to the bulkier pyrene molecule. The importance of molecular sieving for the sorption capacity of carbonaceous sorbents has previously been recognized (*33*, *34*).

The maximum amount of PAHs in a monolayer covering a smooth surface was estimated from the molecular surface area of the molecules (*35*). The estimated monolayer sorption capacity for phenanthrene and pyrene is 1.7×10^{-6} and 1.6×10^{-6} mol per m^2 of surface, respectively, which are within the range of the K^*_{Fr} values reported in Table 2. These estimates suggest that the accessible internal surface areas of coke and AC are completely covered with phenanthrene and pyrene at the solubility limit of these PAHs. Furthermore, a normalization of K^*_{Fr} by the total meso- and micropore volume show that a significant portion of the total micro- and mesopore space is filled with PAHs at the solubility limit. Thus, at the solubility limit of PAHs, the solid−water interface of coke and activated carbon appears to resemble the pure PAH solid.

Table 2 contains literature data of isotherm parameters measured for the same solutes and similar sorbents for comparison. After normalization by the BET-SA, the various K^*_{Fr} values agree within a factor of 2−3 for each PAH compound with the exception of the phenanthrene data reported by Kleineidam et al. (*36*) for F100 activated carbon. The various Freundlich isotherms are compared in Figure S5 in the Supporting Information. Sorption isotherms for PAHs and other black carbon materials or soots are also reported in refs *14*, *33*, and *37*.

Sorption Kinetics: Batch Experiments. Figure 2 presents the time-dependent, apparent sorption distribution coefficient measured as a function of time in batch experiments as observed for phenanthrene (Figures 2a, 2c, and 2e) and pyrene (Figures 2b, 2d, and 2f) with two sieve fractions of POM (1−1.4 and 2−2.8 mm), coke (0.06−0.1 and 0.1−0.25 mm), and AC (0.06−0.25 and 1−2 mm). For POM as a sorbent and phenanthrene as a solute, the coarser sieve fraction approaches the same apparent $K_{d,long\text{-}term}$ as the finer sieve fraction after approximately 180 days, and the final $K_{d,long\text{-}term} = 5300 \pm 1200$ L/kg for the finer fraction is not significantly different from the $K_{d,eq} = 4700 \pm 300$ L/kg derived from the sorption isotherm. Apparently phenanthrene reaches sorption equilibrium within 26 weeks in batches with the coarser POM beads. For pyrene as the solute, the finer POM sieve fraction reaches a $K_{d,long\text{-}term} = 12000 \pm 800$ L/kg close to the $K_{d,eq} = 12000 \pm 1000$ L/kg after 6 weeks, whereas for the coarser POM the measured $K_{d,long\text{-}term}$ of pyrene approaches the equilibrium value derived from the sorption isotherms, although it is not attained during the 30 weeks of the experiment.

For the experiments with coke, both solutes and both sieve fractions reached an apparent steady state within the time frame of the experiment as shown in Figures 2c and 2d. The $K_{d,long\text{-}term}$ values from the kinetic sorption experiments are less than the $K_{d,eq}$ values derived from the sorption isotherms with pulverized coke as shown in Figures 2c and 2d and reported in Table 3. Furthermore, $K_{d,long\text{-}term}$ values derived from the sorption kinetic tests are particle-size-dependent with finer-size coke particles showing greater values of $K_{d,long\text{-}term}$. Thus, the particle-size-dependent variation in the BET-SA and the meso- and micropore volume reported in Table 2 for coke results in a distinct difference in the observed apparent steady state and the resulting measured values of $K_{d,long\text{-}term}$ in the sorption kinetic tests. Better agreement between the kinetic experiment and the isotherm data is obtained if both $K_{d,long\text{-}term}$ and $K_{d,eq}$ are normalized by the BET-SA for the coarse and fine coke particles as shown in Table 3.

For AC, none of the sorption kinetic test results with millimeter-sized AC reached the sorption equilibrium or an apparent steady state within the time frame of the experiment as shown in Figures 2e and 2f. The aqueous PAH concentration fell quickly below the detection limit of the fluorescence method in the batches with the finer AC, and the apparent values of K_d in these batches could only be determined for the first few days. For the coarser AC particles (1−2 mm), the apparent K_d increases continuously during the 200 days of the experiment. From the respective sorption isotherms, one estimates a $K_{d,eq}$ of 3×10^{10} for phenanthrene and 8×10^{10}

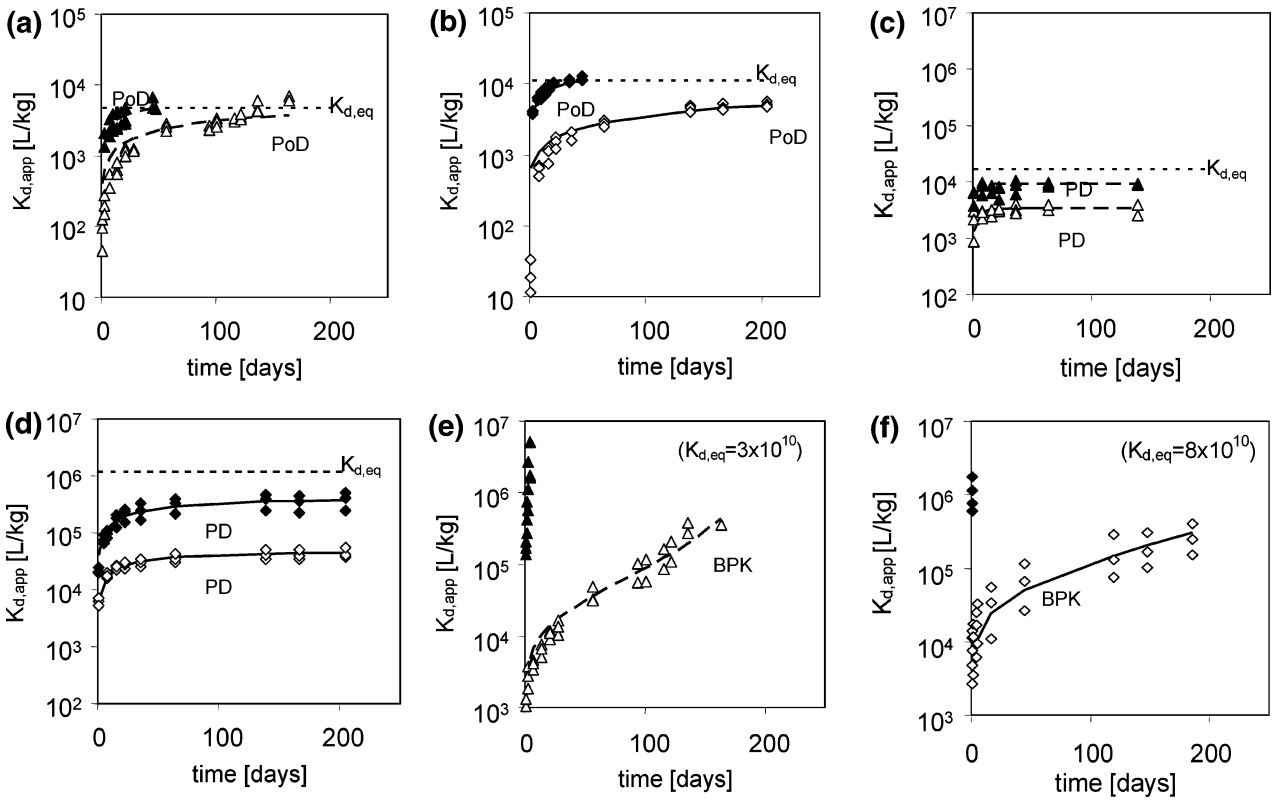

FIGURE 2. Kinetic sorption experiments for phenanthrene (triangles) and pyrene (diamonds) for polyoxymethylene (a and b), coke (c and d), and activated carbon (e and f). Filled symbols represent data for the finer particle size. The particle diameters were 1−1.4 and 2−2.8 mm for polyoxymethylene, 0.11−0.25 and 0.06−0.11 mm for coke, and 1−2 and 0.06−0.25 mm for activated carbon. Lines through the data points represent the model fit, where PoD denotes polymer diffusion, PD denotes pore diffusion, and BPK denotes the branched pore kinetic model. Also shown in the figures are the equilibrium $K_{d,eq}$ values for the batch systems calculated from the sorption isotherms, which for activated carbon requires extrapolation to the sub-ng/L range.

TABLE 3. Kinetic Modeling Results

polyoxymethylene (POM), polymer diffusion model

particle size	compound	D_{POM}[a] (cm^2 s^{-1})	steady-state $K_{POM,long-term}$ (cm^3 g^{-1})	$K_{POM,eq}$[b] (cm^3 g^{-1})
coarse	phenanthrene	1×10^{-10}		
fine	phenanthrene	2×10^{-10}	5.3×10^3	4.7×10^3
coarse	pyrene	2×10^{-11}		
fine	pyrene	2×10^{-10}	1.2×10^4	1.2×10^4

coke, intraparticle diffusion model (*19*)

particle size	compound	D_a[a] (cm^2 s^{-1})	steady-state $K_{d,long-term}$ (cm^3 g^{-1})	$K_{d,eq}$[b] (cm^3/g)	steady-state $K_{d,long-term}$ (cm^3/cm^2 BET-SA)	$K_{d,eq}$[b] (cm^3/cm^2 BET-SA)
coarse	phenanthrene	1.2×10^{-11}	3.4×10^3	1.7×10^4	0.16	0.28
fine	phenanthrene	6.5×10^{-12}	9.1×10^3		0.30	
coarse	pyrene	1.2×10^{-12}	4.5×10^4	1.2×10^6	2.0	19
fine	pyrene	1.4×10^{-13}	3.9×10^5		13	

activated carbon, branched pore kinetic model (*28*)

particle size	compound	D_s[a] (cm^2 s^{-1})	f	k_f (s^{-1})	K^*_{fr} (g/g)	1/n
coarse	phenanthrene	2×10^{-11}	0.02	6×10^{-9}	0.34	0.27
coarse	pyrene	3×10^{-12}	0.03	8×10^{-10}	0.13	0.34

[a] For comparison, diffusion coefficients derived from desorption experiments with petrolatum, transmission oil, and paraffin ranged from 1×10^{-9} to 1×10^{-11} for phenanthrene and from 1×10^{-10} to 1×10^{-12} for pyrene (*40*), 6×10^{-15} and 3×10^{-15}, respectively, for solidified tar decanter sludge (*41*), and 1×10^{-16} to 1×10^{-17} and 1×10^{-17} to 1×10^{-18}, respectively, for coal-derived sediment particles (*16*). [b] Calculated from sorption isotherms for comparison.

for pyrene for the batch systems. This calculation requires, however, extrapolation of the Freundlich isotherm to aqueous solute concentrations far below the range of its experimental validation. The value of $K_{d,eq}$ was calculated based on the mass balance for the kinetic experiment and the isotherm parameters obtained at higher concentrations. This value

was extrapolated to a very low aqueous concentration (e.g., approximately 0.1 ng/L for phenanthrene) and it cannot be used to calculate solid loading at higher concentrations (e.g., ug/L) without considering isotherm nonlinearity.

μL^{2}MS Measurements. These tests were designed to observe the penetration of the PAH molecules into POM, coke, and AC. POM particles were harvested after 10 weeks from 14-mL batches with an initially nearly saturated aqueous solution of phenanthrene and sectioned across the center for μL^{2}MS analysis. An example of a sectioned POM particle (2−2.8 mm) is shown in Figure 3a. The μL^{2}MS mass spectrometer signal intensity for the molecular mass of phenanthrene is shown in Figure 3b as gray symbols, and average intensities from the particle edge to its center are shown as white symbols. The signal intensity resembles the concentration profiles anticipated by spherical diffusion models in which a concentration wave is migrating to the particle center from each edge. As observed, the diffusion front has not yet reached the center of the POM particle. This finding is in agreement with the results of the batch experiments in Figure 3a, where the apparent K_d of coarser POM is still increasing after 70 days, indicating continued uptake of phenanthrene into the POM.

Figure 3c shows a razor-cut coke particle (2−3 mm) that was embedded in cement after 16 weeks of continuous rotation in a batch with an initially nearly saturated aqueous solution of phenanthrene. The μL^{2}MS data show that phenanthrene was detected throughout this particle. The data exhibit a significant scattering with no obvious radial trend in the signal intensity as shown by the gray symbols and the smoother average signal intensities shown as white symbols in Figure 3d. Apparently the radial diffusion of phenanthrene in coke has reached the particle center after 16 weeks. These results are in agreement with the steady-state $K_{d,long\text{-}term}$ values observed for smaller-size coke particles within a few days after the start of the batch sorption experiments (Figure 2c). The image in Figure 3c shows plaster penetrating the macropores in the interior of the cut coke particle, which indicates a direct access route for the sorbing solute. The resolution of the μL^{2}MS laser is insufficient to distinguish between macroporous and meso- or microporous regions within the cut coke particle. Thus, the signal intensities measured by μL^{2}MS represents an average of the phenanthrene concentration of macroporous, microporous, and polymeric domains.

Figure 3e shows a razor-cut AC particle (1−2 mm) embedded in cement after 16 weeks of continuous rotation in the batch test with an initially nearly saturated solution of phenanthrene. In this case, phenanthrene was detected with much higher signal intensity at the edge of the particle as shown by the gray and white symbols in Figure 3f. As observed, the radial diffusion of phenanthrene inside AC is slow compared to that of POM or coke. These results are corroborated by the continuous increase of the values of apparent K_d during 200 days of monitoring in the batch kinetic experiments as shown in Figure 2e.

In a time series of similar experiments, POM and AC particles were exposed in 40-mL batches to an initially nearly saturated aqueous solution of both phenanthrene and pyrene. The particles were razor-cut across the particle center after exposure without embedment. These data are shown in Figure 4, which illustrates the average signal intensity in the radial direction from the particle edge to the particle center relative to the signal intensity measured on the exterior surface. For POM, the broadening of the diffusion front is observed with increasing time, and phenanthrene diffuses faster than pyrene, as shown in Figures 4a, 4c, 4e, and 4g. The signal intensity of phenanthrene is nearly homogeneous throughout the POM particle after 34 weeks, whereas pyrene clearly has not yet reached sorption equilibrium. These results are in good agreement with the prior observations in the batch experiments shown in Figures 2a and 2b. In the corresponding measurements with AC shown in Figures 4b, 4d, 4f, and 4h, phenanthrene and pyrene were always detected with higher intensity in the exterior region of the particles compared to the interior. This behavior indicates that most of the PAH mass is located within 80−200 μm from the exterior surface, an area covered by two to five adjacent laser-desorption measurements. In addition, PAHs are detected at a low intensity throughout the AC particles without an obvious radial trend. These smaller signals indicate faster spreading of a fraction of the total PAHs throughout the particle center along preferential diffusion pathways.

The concentration dependency of the radial diffusion in POM and AC (*38*) was also investigated with μL^{2}MS, and the air-bridge system and is discussed in Figure S6 in the Supporting Information. For POM particles, the intraparticle diffusion appears to be independent of the PAH concentration. For AC, the radial diffusion of phenanthrene and pyrene is significantly faster at higher aqueous PAH concentrations.

Modeling Results. The results of our sorption kinetic experiments with PAHs and POM can be explained by the classic polymer diffusion model for spherical geometries. For polymer diffusion, the governing equation of contaminant diffusion in a homogeneous spherical particle can be written in the form

$$\frac{\partial q_{poly}}{\partial t} = \frac{D_{poly}}{r^2}\frac{\partial}{\partial r}\left(r^2\frac{\partial}{\partial r}q_{poly}\right) \quad (2)$$

where t denotes the time, r the radial distance from the particle or aggregate center, q_{poly} (g/g) is the concentration of the PAH in the polymer, and D_{poly} (cm^2/s) the diffusion coefficient of the PAH in the polymer. We neglect external mass transfer resistance and assume that the PAH concentration $q_{poly}(R)$ on the external surface of the polymer particle is in a linear partitioning equilibrium with the surrounding water phase.

$$q_{poly}(R) = K_{poly}C_w \quad (3)$$

where R denotes the particle radius and K_{poly} (cm^3/g) the linear partitioning coefficient between the polymer and the aqueous phase. Although the external mass transfer resistance may be important during initial sorptive uptake, the assumption is considered appropriate because the kinetic tests were performed over a long-term period of more than 200 days, and the lower $K_{d,app}$ values from the early-time data have less weight in data analysis. The complete boundary and initial conditions are given as Supporting Information. We described the POM sorption kinetic data from the batch experiments with a numerical technique based on the polymer diffusion model, using in eq 2 the steady-state value of $K_{POM,long\text{-}term}$ from Table 3. Polymer diffusion coefficients D_{poly} were obtained as the fitting parameter from the kinetic sorption experiment data in Figures 2a and 2b, by minimizing the squared residuals between model prediction and data. The fitted D_{poly} values are listed as D_{POM} in Table 3. The model fit is shown in Figures 2a and 2b for phenanthrene and pyrene, respectively. For phenanthrene, the fitted D_{POM} values of the two size fractions agree. The fitted D_{POM} of the finer sieve fraction is approximately a factor 2 larger, which could be explained by a larger external surface to volume ratio of the cut particles. Razor-cut particles were not as well-rounded as the original-size resin and had a rough surface because of some internal, bubblelike cavities in the POM, which could facilitate the uptake initially. For pyrene, the fitted D_{POM} values vary by a factor of 10 for the two size fractions. The value for the finer POM fraction seems unusually high, especially when

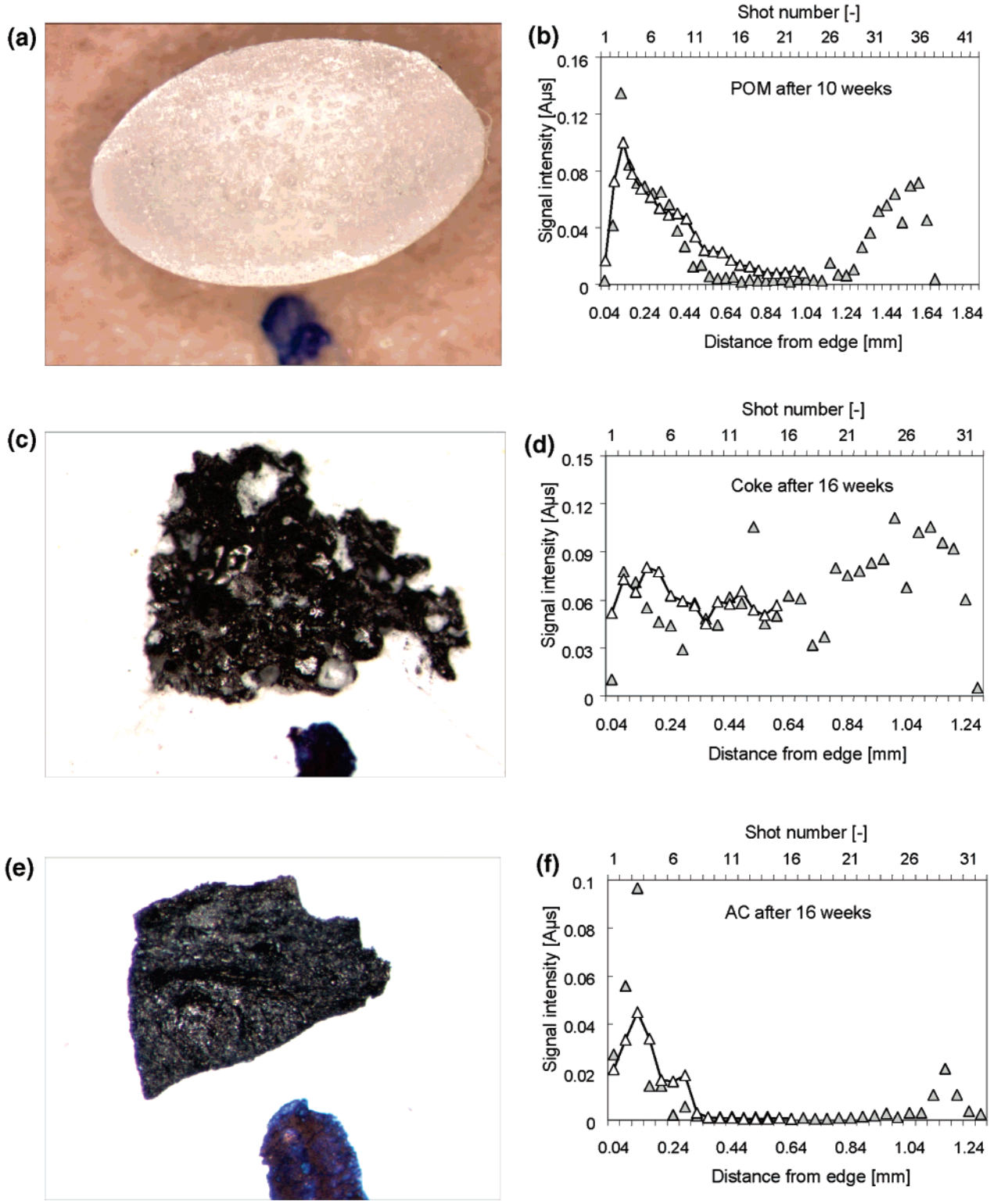

FIGURE 3. Images and μL^2MS measurements for polyoxymethylene (a and b), coke (c and d), and activated carbon (e and f) exposed to an initially nearly saturated phenanthrene solution in a closed batch system. The filled triangles show a concentration profile measured with μL^2MS on an embedded and sectioned particle shown in the adjacent image. Consecutive shots are approximately 40 μm apart and taken along a line from the particle edge across the particle center to the opposite edge. Empty triangles show average values for shots equidistant from the outer surface of the particle. Averages were calculated from three cross sections measured on different particles. Because of the current limitation of the instrument resolution, the first shot of the laser beam is often partially on the particle surface and partially outside the particle surface resulting in low signal intensity for the first shot.

compared to the respective D_{POM} of phenanthrene. No explanation could be found for this observation.

The numerical model was used to predict the radial PAH concentration profile within the coarse POM particles for the batch experiments, and the predicted concentration profiles are compared with the μL^2MS data in Figures 4a, 4c, 4e, and 4g. The concentrations were normalized by the predicted concentration on the external surface for the

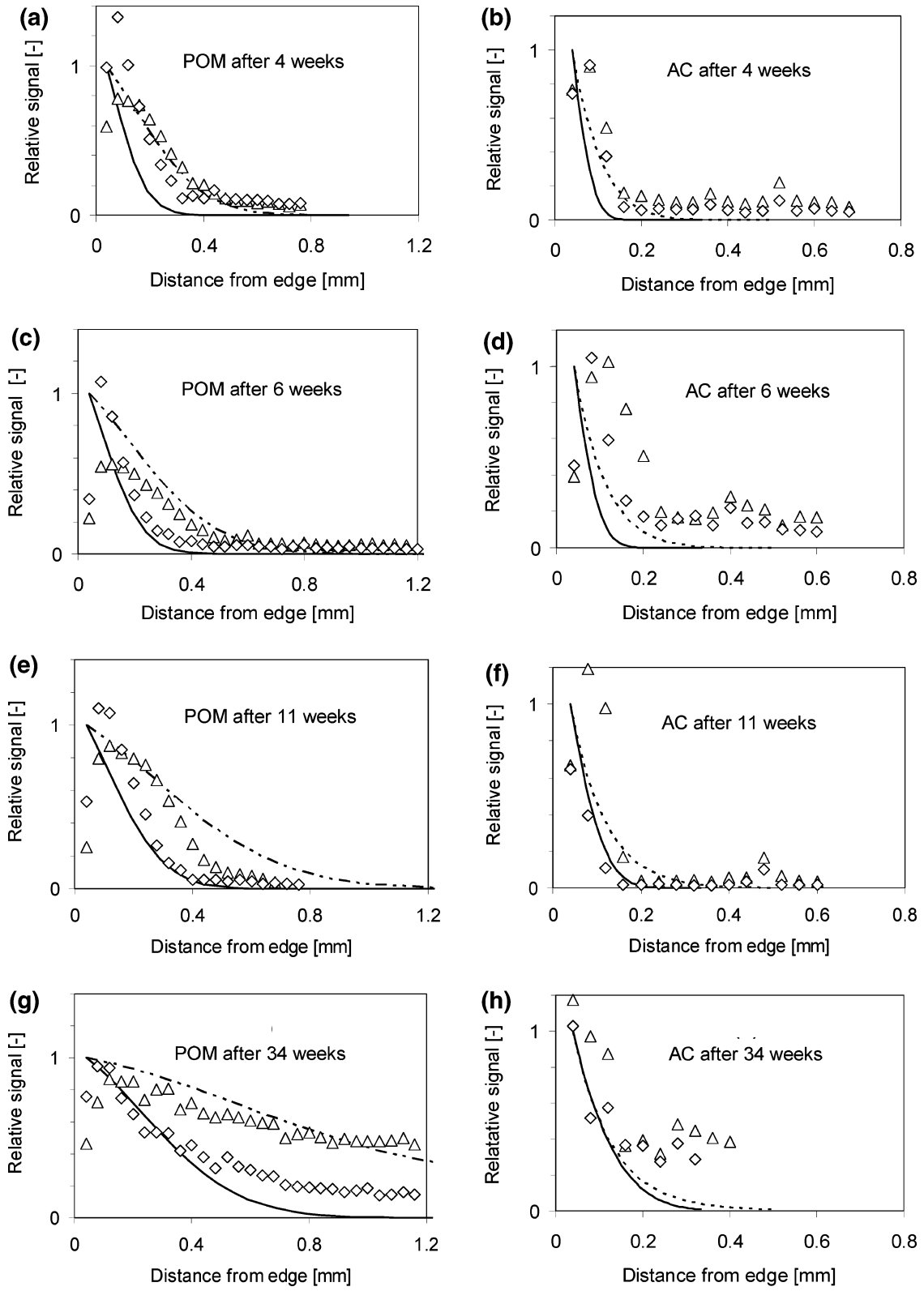

FIGURE 4. **μL^{2}MS measurements for polyoxymethylene (a, c, e, and g) and activated carbon (b, d, f, and h), showing the phenanthrene (triangles) and pyrene (diamonds) molecular mass signals inside sectioned particles as a function of the distance from the outer surface and time. Shown are average values for shots equidistant from the outer surface of the particle, calculated from three profiles measured across the center of the same particle. Each particle was enclosed in a batch with 40 mL of water initially nearly saturated with phenanthrene and pyrene. Signal intensity is normalized by the average intensity measured as a 50-shot average on the exterior surface of the same particle. μL^{2}MS measurements are compared with the concentration profiles predicted from the diffusion models shown as solid or broken lines. Note that these lines have not been fitted to the μL^{2}MS data. The first shot of the laser beam is often partially on the particle surface and partially outside the particle surface resulting in low signal intensity.**

comparisons, and the distance between data points from the laser shots was set equal to 40 μm. The agreement between the predicted PAH concentration profiles and the measured μL^{2}MS data is reasonably good as shown in Figures 4a, 4c,

4e, and 4g. The deviation between model predictions and μL^2MS data can probably be explained by scatter in the experimental data and simplifying assumptions such as the spherical particle geometry. Note that no fitting to the μL^2-MS data is involved. We conclude that the spherical polymer diffusion model provides an adequate description for the sorption kinetics and diffusion of PAHs in a relatively homogeneous and approximately spherical rubbery polymer such as POM.

The sorption kinetics of PAHs in batches with coke particles were interpreted using an intraparticle diffusion model for porous sorbents described by Ball and Roberts (*19*). This model assumes a linear reversible partitioning equilibrium within the pore space and spherical geometries. The governing equation of contaminant diffusion in a homogeneous spherical particle is written in the form

$$\frac{\partial C_{pw}}{\partial t} = \frac{D_a}{r^2}\frac{\partial}{\partial r}\left(r^2\frac{\partial}{\partial r}C_{pw}\right) \quad (4)$$

where D_a (cm^2/s) denotes an apparent diffusion coefficient and C_{pw} (g/cm^3) the pore water concentration of the diffusing PAH. The apparent diffusion coefficient D_a accounts for pore diffusion, and surface diffusion and can be interpreted as (*19*)

$$D_a = \frac{\epsilon}{\epsilon + \rho K_d}D_p + \frac{\rho K_d}{\epsilon + \rho K_d}D_s \quad (5)$$

where ϵ denotes the porosity of the sorbent, ρ the bulk density of the sorbent, K_d the linear solid−water distribution coefficient, D_p the pore diffusion coefficient, and D_s the surface diffusion coefficient. External mass transfer resistance was neglected. Boundary and initial conditions are given as Supporting Information.

The distribution of the PAHs between the water and the solid phase was described by the steady-state $K_{d,long\text{-}term}$ from the batch kinetic experiments, $K_d = K_{d,long\text{-}term}$, reported in Table 3. Because the solid−water distribution for coarse and fine particles could not be predicted from the isotherm data for pulverized coke, it was important to use the endpoint of the kinetic experiment, $K_{d,long\text{-}term}$, to account for the particle-size dependence on the apparent distribution coefficient at steady state observed for the batch experiments. The aqueous PAH concentrations in the batch experiments with coke particles were observed to decrease by less than an order of magnitude, and thus the assumption of a concentration-independent $K_d = K_{d,long\text{-}term}$ is a reasonable first approximation, despite the nonlinearity of the sorption isotherm in Figure 1b. The fitted D_a values are compiled in Table 3, and the model fit is shown by the broken or solid lines in Figures 2c and 2d for phenanthrene and pyrene, respectively. The fitted apparent diffusivity is greater for phenanthrene as compared to that of pyrene as well as greater for the coarser coke particle size. This result is explained by the intraparticle diffusion model if sorption-retarded pore diffusion dominates and the surface diffusion coefficient is negligible in eq 4. The apparent diffusivity should then be approximately inversely proportional to K_d. The ratio of the measured apparent steady-state $K_{d,long\text{-}term}$ is indeed approximately inversely proportional to the ratio of the corresponding D_a values in Table 3. Thus, the intraparticle diffusion model for porous sorbents described by Ball and Roberts (*19*) can rationalize the kinetic sorption data for batch experiments with coke particles if one allows for a particle-size-dependent sorption capacity in the pore space. It is possible that sorption to coke occurs as a two-step process with a comparatively fast initial diffusion into the readily accessible pore space over 10−30 days, as observed in Figures 3c and 3d, followed by a secondary, much slower uptake, which was not apparent over the time frame of our kinetic experiments.

The sorption kinetics of PAHs in batches with AC particles were evaluated with the intraparticle diffusion model and with a modified version of the pore diffusion model described by Grathwohl (*20*), which uses the nonlinear Freundlich sorption isotherm to describe the local solid−water partitioning equilibrium. These models predicted that diffusion would occur only within the outermost 40 μm (one μL^2MS laser shot) of the AC particle during the entire duration of the kinetic experiments. These predictions clearly do not agree well with the μL^2MS measurements in Figures 3f, 4b, 4d, 4f, and 4h. Therefore, the branched pore kinetic model of Peel and Benedek (*28*) was used to interpret the data. The branched pore kinetic model divides the particle volume into a macroporous and a microporous domain. Radial diffusion occurs along the macropore walls by surface diffusion, and the kinetics of the exchange of chemicals between the macroporous and the microporous domain is described by a gradient flux law. The relevant equations are

$$f\frac{\partial q_s}{\partial t} = f\frac{D_s}{r^2}\frac{\partial}{\partial r}\left(r^2\frac{\partial}{\partial r}q_s\right) - k_f(q_s - q_b) \quad (6)$$

$$(1-f)\frac{\partial q_b}{\partial t} = k_f(q_s - q_b) \quad (7)$$

where f is the fraction of the particle pore volume filled by the macropores and $(1-f)$ is the fraction of the particle pore volume occupied by micropores, q_s (g/g) denotes the solid-phase PAH concentration in the macroporous domain, q_b (g/g) denotes the solid-phase PAH concentration in the microporous domain, and k_f (s^{-1}) is the kinetic exchange rate between macro- and microporous domains. This model neglects an eventual PAH mass in the pore water. External mass transfer resistance was considered negligible, and the external boundary condition was determined from the partitioning equilibrium between the PAH concentration in the batch water and the solid phase of the macroporous domain as described by the Freundlich isotherm in eq 1. Initial and boundary conditions are provided as Supporting Information. The three parameters f, D_s, and k_f were determined from a multiparameter fit to the apparent K_d data in Figures 2e and 2f with a least-squares residuals procedure. Model input parameters and fitted parameters are listed in Table 3. The model describes the kinetic data well, as shown by the solid and broken lines in Figures 2e and 2f for phenanthrene and pyrene, respectively. The predicted radial PAH concentration profiles inside AC particles are compared with the μL^2MS data in Figures 4b, 4d, 4f, and 4h. The branched pore kinetic model predicts a spreading of the PAHs over a distance of 200−400 μm. This is in better agreement with the μL^2MS data than for predictions based on the assumption of a single homogeneous sorption domain. Therefore, it appears that PAHs diffuse radially along preferential pathways, presumably macropores. A kinetic exchange of PAHs between macroporous and microporous domains occurs in parallel. While the branched pore kinetic model is in better agreement with the experimental data, a number of parameter combinations f, k_f, and D_s could provide a similar fit to the experimental batch data. There is currently no established procedure for determining each of these parameters separately and no obvious way of distinguishing the two sorption domains within the particles. The fitted volume fraction, f, occupied by the "macropores" is much smaller than the difference between the total and the meso- and micropore volume of AC reported in Table 2. Peel et al. (*28*) stress for their model that the regions comprising different diffusion rates should not be confused with the conventional use of the terms to

define a certain range of pore sizes. The low values for f determined in this study indicate that this parameter may represent the fraction of the total sorption capacity in the macropore region rather than the macropore volume. The sorption capacity of the macropores is expected to be less than that of mesopores or micropores, because of the lower surface area to pore volume ratio. The branched pore diffusion model does not account for the concentration dependency of the radial diffusivity D_s, and the fitted parameter values in Table 3 are only valid for the solute concentration range used in the experiment.

This work illustrates how physical characteristics, such as the BET-SA and the meso- and microporosity, of a carbonaceous sorbent relate to sorption capacity and how both physical characteristics and the sorption capacity affect the kinetics of sorption. This work also demonstrates how techniques such as μL^2MS can help confirm modeling assumptions and model parameters by providing spatially resolved concentration profiles within particles. While our results confirm many of the qualitative predictions of diffusion-based sorption models, we also demonstrate the complexity of the actual diffusion process, especially for coke and activated carbon. The reasonably good fit obtained for many kinetic sorption data by simple diffusion-based models does not necessarily prove the details of the underlying kinetic mechanism, and model extrapolations beyond the range of empirical validation, i.e., estimated times to equilibrium, need to acknowledge this uncertainty.

Acknowledgments

The equilibrium and kinetic batch experiments were conducted at the Laboratory of Water and Air Analysis, Department of Environment, University of the Aegean. We also thank Eleni Iliopoulou and Irene Klontza for technical assistance in the laboratory. Support was provided by the Department of Defense through the Strategic Environmental Research and Development Program (Contract No. DACA72-01-C-0002). Supplemental funding was provided by the Ford Fund. Dr. David Werner received support from the Swiss National Science Foundation (Grant No. 81EL68477).

Supporting Information Available

Detailed method description, figures, numerical models, and annotation. This material is available free of charge via the Internet at http://pubs.acs.org.

Literature Cited

(1) Sontheimer, H.; Crittenden, J. C.; Summers, R. S. *Activated Carbon for Water Treatment*, 2nd ed.; DVGW−Forschungsstelle Engler-Bunte-Institut Universitat Karlsruhe (TH): Karlsruhe, Germany, 1988.

(2) Karapanagioti, H. K.; Sabatini, D. A. Impacts of heterogeneous organic matter on phenanthrene sorption: Different aquifer depths. *Environ. Sci. Technol.* **2000**, *34*, 2453−2460.

(3) Talley, J. W.; Ghosh, U.; Tucker, S. G.; Furey, J. S.; Luthy, R. G. Particle-scale understanding of the bioavailability of PAHs in sediment. *Environ. Sci. Technol.* **2002**, *36*, 477−483.

(4) Ghosh, U.; Zimmerman, J. R.; Luthy, R. G. PCB and PAH speciation among particle types in contaminated harbor sediments and effects on PAH bioavailability. *Environ. Sci. Technol.* **2003**, *37*, 2209−2212.

(5) Grathwohl, P.; Peschik, G. In *International Conference on Containment Technology*; St. Petersburg, FL, 1997.

(6) Zimmerman, J. R.; Ghosh, U.; Millward, R. N.; Bridges, T. S.; Luthy, R. G. Addition of carbon sorbents to reduce PCB and PAH bioavailability in marine sediments: Physicochemical tests. *Environ. Sci. Technol.* **2004**, *38*, 5458−5464.

(7) Zimmerman, J. R.; Werner, D.; Ghosh, U.; Millward, R. N.; Bridges, T. S.; Luthy, R. G. The effects of dose and particle size on activated carbon treatment to sequester polychlorinated biphenyls and polycyclic aromatic hydrocarbons in marine sediments. *Environ. Toxicol. Chem.* **2005**, *24*, 1594−1601.

(8) Werner, D.; Higgins, C. P.; Luthy, R. G. The sequestration of PCBs in Lake Hartwell sediment with activated carbon. *Water Res.* **2005**, *39*, 2105−2113.

(9) Allen-King, R. M.; Grathwohl, P.; Ball, W. P. New modeling paradigms for the sorption of hydrophobic organic chemicals to heterogeneous carbonaceous matter in soils, sediments, and rocks. *Adv. Water Resour.* **2002**, *25*, 985−1016.

(10) Cornelissen, G.; Van Noort, P. C. M.; Govers, H. A. J. Mechanism of slow desorption of organic compounds from sediment: A study using model sorbents. *Environ. Sci. Technol.* **1998**, *32*, 3124−3131.

(11) Rugner, H.; Kleineidam, S.; Grathwohl, P. Long-term sorption kinetics of phenanthrene in aquifer materials. *Environ. Sci. Technol.* **1999**, *33*, 1645−1651.

(12) Xia, G.; Pignatello, J. J. Detailed sorption isotherms of polar and apolar compounds in a high-organic soil. *Environ. Sci. Technol.* **2001**, *35*, 84−94.

(13) Accardi-Dey, A.; Gschwend, P. M. Reinterpreting literature sorption data considering both absorption into organic carbon and adsorption onto black carbon. *Environ. Sci. Technol.* **2003**, *37*, 99−106.

(14) Cornelissen, G.; Gustafsson, O. Sorption of phenanthrene to environmental black carbon in sediment with and without organic matter and native sorbates. *Environ. Sci. Technol.* **2004**, *38*, 148−155.

(15) Karapanagioti, H. K.; Kleineidam, S.; Sabatini, D. A.; Grathwohl, P.; Ligouis, B. Impacts of heterogeneous organic matter on phenanthrene sorption: Equilibrium and kinetic studies with aquifer material. *Environ. Sci. Technol.* **2000**, *34*, 406−414.

(16) Ghosh, U.; Talley, J. W.; Luthy, R. G. Particle-scale investigation of PAH desorption kinetics and thermodynamics from sediment. *Environ. Sci. Technol.* **2001**, *35*, 3468−3475.

(17) Wu, S. C.; Gschwend, P. M. Numerical modeling of sorption kinetics of organic compounds to soil and sediment particles. *Water Resour. Res.* **1988**, *24*, 1373−1383.

(18) Brusseau, M. L.; Jessup, R. E.; Rao, P. S. C. Nonequilibrium sorption of organic chemicals: Elucidation of rate-limiting processes. *Environ. Sci. Technol.* **1991**, *25*, 134−142.

(19) Ball, P. W.; Roberts, V. P. Long-term sorption of halogenated organic chemicals by aquifer material. 2. Intraparticle diffusion. *Environ. Sci. Technol.* **1991**, *25*, 1237−1249.

(20) Grathwohl, P. *Diffusion in Natural Porous Media: Contaminant Transport, Sorption/Desorption and Dissolution Kinetics*; Kluwer: Boston, MA, 1998.

(21) Choi, J. G.; Do, D. D.; Do, H. D. Surface diffusion of adsorbed molecules in porous media: Monolayer, multilayer, and capillary condensation regimes. *Ind. Eng. Chem. Res.* **2001**, *40*, 4005−4031.

(22) Harmon, T. C.; Roberts, P. V. Comparison of intraparticle sorption and desorption rates for a halogenated alkene in a sandy aquifer material. *Environ. Sci. Technol.* **1994**, *28*, 1650−1660.

(23) Farrell, J.; Reinhard, M. Desorption of halogenated organics from model solids, sediments, and soil under unsaturated conditions. 2. Kinetics. *Environ. Sci. Technol.* **1994**, *28*, 63−72.

(24) Arocha, M. A.; Jackman, A. P.; McCoy, B. J. Adsorption kinetics of toluene on soil agglomerates: Soil as a biporous sorbent. *Environ. Sci. Technol.* **1996**, *30*, 1500−1507.

(25) Werth, C. J.; Reinhard, M. Effects of temperature on trichloroethylene desorption from silica gel and natural sediments. 2. Kinetics. *Environ. Sci. Technol.* **1997**, *31*, 697−703.

(26) Bujalski, R.; Cantwell, F. F. Comment on "Direct analysis of intraparticle mass transfer in silica gel using single-microparticle injection and microabsorption methods". *Langmuir* **2001**, *17*, 7710−7711.

(27) Ko, D. C. K.; Tsang, D. H. K.; Porter, J. F.; McKay, G. Application of multipore model for the mechanism identification during the adsorption of dye on activated carbon and bagasse pith. *Langmuir* **2003**, *19*, 722−730.

(28) Peel, R. G.; Benedek, A.; Crowe, C. M. A Branched pore kinetic-model for activated carbon adsorption. *AIChE J.* **1981**, *27*, 26−32.

(29) Verardo, D. J.; Froelich, P. N.; McIntyre, A. Determination of organic carbon and nitrogen in marine sediments using the Carlo Erba NA-1500. *Deep-Sea Res., Part A* **1990**, *37*, 157−165.

(30) Bucheli, T. D.; Gustafsson, O. Quantification of the soot−water distribution coefficient of PAHs provides mechanistic basis for enhanced sorption observations. *Environ. Sci. Technol.* **2000**, *34*, 5144−5151.

(31) Jonker, M. T. O.; Koelmans, A. A. Polyoxymethylene solid-phase extraction as a partitioning method for hydrophobic organic

chemicals in sediment and soot. *Environ. Sci. Technol.* **2001**, *35*, 3742−3748.
(32) Walters, R. W.; Luthy, R. G. Equilibrium adsorption of polycyclic aromatic hydrocarbons from water onto activated carbon. *Environ. Sci. Technol.* **1984**, *18*, 395−403.
(33) Jonker, M. T. O.; Koelmans, A. A. Sorption of polycyclic aromatic hydrocarbons and polychlorinated biphenyls to soot and soot-like materials in the aqueous environment: mechanistic considerations. *Environ. Sci. Technol.* **2002**, *36*, 3725−3734.
(34) Van Noort, P. C. M.; Jonker, M. T. O.; Koelmans, A. A. Modeling maximum adsorption capacities of soot and soot-like materials for PAHs and PCBs. *Environ. Sci. Technol.* **2004**, *38*, 3305−3309.
(35) Werner, D.; Karapanagioti, H. Comment on "Modeling Maximum Adsorption Capacities of Soot and Soot-like Materials for PAHs and PCBs". *Environ. Sci. Technol.* **2004**, *39*, 381−382.
(36) Kleineidam, S.; Schuth, C.; Grathwohl, P. Solubility-normalized combined adsorption-partitioning sorption isotherms for organic pollutants. *Environ. Sci. Technol.* **2002**, *36*, 4689−4697.
(37) James, G.; Sabatini, D. A.; Chiou, C. T.; Rutherford, D.; Scott, A. C.; Karapanagioti, H. K. Evaluating phenanthrene sorption on various wood chars. *Water Res.* **2005**, *39*, 549−558.
(38) Chang, C. F.; Chang, C. Y.; Holl, W.; Ulmer, M.; Chen, Y.-H.; Gross, H. J. Adsorption kinetics of polyethylene glycol from aqueous solution onto activated carbon. *Water Res.* **2004**, *38*, 2559−2570.
(39) Mackay, D.; Shiu, W. Y.; Ma, K. C. *Illustrated Handbook of Physical-Chemical Properties and Environmental Fate for Organic Chemicals*; Lewis Publishers: Chelsea, MI, 1992; Vol. 2.
(40) Ortiz, E.; Kraatz, M.; Luthy, R. G. Organic phase resistance to dissolution of polycyclic aromatic hydrocarbon compounds. *Environ. Sci. Technol.* **1999**, *33*, 235−242.
(41) Ahn, S.; Werner, D.; Luthy, R. G. Physicochemical characterization of coke plant soil for the assessment of polycyclic aromatic hydrocarbons availability and the feasibility of phytoremediation. *Environ. Toxicol. Chem.* **2005**, *24*, in press.

Received for review January 17, 2005. Revised manuscript received June 16, 2005. Accepted June 16, 2005.

ES050113O